ICARUS 82, 167–179 (1989)

Mass Transfer during Ice Particle Collisions in Planetary Rings[1]

J. S. B. MCDONALD,* A. HATZES,† F. BRIDGES,* AND D. N. C. LIN†

*Board of Studies in Physics and †Board of Studies in Astronomy and Astrophysics, University of California, Santa Cruz, California 95064

Received August 12, 1988; revised March 17, 1989

The collisional properties of ice particles determine the structure and dynamical evolution of planetary rings as well as the particle-size distribution. In this contribution, we present experimental data on the mass transfer during ice particle collisions in a laboratory environment which partially simulates the conditions in planetary rings. These data indicate that the interacting volume depends on the impact velocity. During a collision, the fraction of this volume exchanged is quite small, ~5%; however, the net amount of material transferred may be considerably smaller. We discuss the possible implication of these data on the structure and dynamical evolution of planetary rings. © 1989 Academic Press, Inc.

I. INTRODUCTION

The collisional properties of constituent particles play important roles in the structure and dynamical evolution of planetary rings. For example, the velocity dispersion of the particles and the thickness of the rings are determined by the coefficient of restitution (ε) of ring particles (Goldreich and Tremaine 1978). Experimentally determined values of ε for direct impact between particles with smooth surfaces (Bridges *et al.* 1984) provide estimates for the thickness of the rings (~10 m) which are consistent with Voyager's data (Marouf *et al.* 1983). The corresponding value of the velocity dispersion is ~0.1 cm sec^{-1}. A recent comprehensive analysis (Hatzes *et al.* 1988, hereafter Paper 1) indicates that ε is also dependent upon the particle surface structures; collisions between particles with frosty surfaces are more dissipative. In general, collisions modify the surface structure of the contact region and induce mass transfer between colliding particles, the extent of which is dependent upon the impact velocity and surface roughness. In this contribution, we present experimental data on mass transfer for direct collisions to establish constraints on surface properties and the size distribution of ring particles. We also contrast the collisional effects with accretion of micron-size ice grains which are observed to have optical depth up to ~0.1 in Saturn's rings (Cuzzi *et al.* 1984). If the accreted grains form a frost layer on the surface, collisions will continually compact the surface layer while mass transfer proceeds.

The experimental procedure is described in Section II. Section III outlines the experimental results and their implication and Section IV contains application of the data to planetary rings.

II. EXPERIMENTAL APPARATUS AND PROCEDURE

(a) *Mechanical Setup*

The experimental apparatus and procedure are described in detail in Paper 1. We utilize a compound pendulum to simulate collisions between a small ice sphere (with a radius of 2.5 cm) and a massive particle with infinite radius (an ice brick with a flat surface secured to a 12-kg lead brick), and for a range of impact velocities (0.5 and 2.0

[1] Lick Observatory Contribution No. 462

0019-1035/89 $3.00

cm sec^{-1}) relevant to ring systems. The small particle is attached to the pendulum, giving it an effective mass of 450 g. Figure 1 in Paper 1 shows a schematic of the pendulum viewed along its rotational axis. In order to simulate the ring environment, the entire assembly is mounted inside a low-temperature cryostat. These measurements were made between 100 and 150°K in an ambient pressure of 760 Torr. The atmosphere is composed of nitrogen gas, free of water vapor in order to minimize frost accumulation on particle surfaces. The collisional properties are independent of the atmospheric pressure (Paper 1); therefore, we assume the presence of this atmosphere does not significantly affect mass transfer.

(b) Preparation of Ice Particles

A major uncertainty in the simulation of particle collisions in planetary rings context is the nature of the surface structure of the particles. Low velocity collisions compact loose ice chips in the regions of contact and lead to smooth surfaces whereas high velocity collisions and micrometeorite impacts introduce fracture and dislocation. In order to examine the dependence of mass transfer rate on the surface structure, we prepared the particles with two limiting surface conditions: (1) very smooth surfaces and (2) roughened surfaces with a characteristic length scale, l_c, for irregular surface structure that is larger than the contact area. We utilize three methods to estimate the magnitude of the radius of the contact area, r. First, we adopt a theoretical estimate based on Hertz's law for elastic collisions (Borderies *et al.* 1984) such that $r/R \simeq (\rho v^2/E)^{0.2}$, where R and ρ are the radius and density of the ice particle, respectively, v is the velocity of impact, and E is the elastic modulus. At the appropriate temperatures $E \sim 10^{11}$ dyn cm^{-2} for water ice (Hobbs 1974) so that $r \sim 0.01$ cm for particles with $R = 2.5$ cm and $v \simeq 0.5$ cm sec^{-1}. This value is a lower limit on r since structural changes during contact increase the contacting surface. We can also determine another limit on r from the amount of mass transferred during the first few collisions between ice particles with smooth surfaces. During contact, the maximum volume in the compressed region is $\sim Dr^2$, where $D \sim r^2/R$ is the maximum compressional depth. If a significant fraction of the material in the compressed volume is transferred, we would deduce from the data in Section III that $r \sim 0.02$ cm. A third method which yields an upper limit on r is based on the high resolution measurements of the particles' position as a function of time during contact (Paper 1). Correcting for instrumental response, we can directly estimate an upper limit on D (Paper 1) and obtain $r \sim 0.03$–0.05 cm for $v \simeq 0.5$ cm sec^{-1}.

Collisions between particles with irregular surface features that have a length scale larger than r (and therefore, on the scale of r, the contact area is smooth) are unlikely to differ significantly from those between smooth particles. Surface variations with a length scale much smaller than r are also unlikely to strongly affect mass transfer due to the collisions. Based on the above estimates, we introduced irregular features and variations in the radius of curvature by brushing the impact surfaces with a fine wire brush with spacing between the wires less than 0.1 cm. Using this method, we produced irregular structures with a characteristic length scale ~ 0.02–0.04 cm and a depth scale of ~ 0.01–0.03 cm.

In order to determine the amount of mass transfer, we prepared one of the two colliding ice particles with a fluorescent dye. After a specified number of collisions, the amount of dye transfer is determined with a spectral fluorimeter, an apparatus which measures the fluorescence intensity as a function of wavelength of a material excited by ultraviolet radiation. The sensitivity of this equipment is sufficient to measure concentrations as low as 5×10^{-10} moles per liter, which corresponds to $\sim 10^{-7}$ g of ice transferred (see Section III).

The best results for this experiment were obtained using fluorescein, which has a

peak emission at 511 nm. One of the two ice particles is prepared using a high concentration of the dye (10^{-3} moles per liter, or 0.38 g of dye per liter), the other is prepared with distilled, filtered, and deionized water to minimize fluorescence contamination. In our experiment, we measured the amount of fluorescent dye transferred, and calculated the corresponding amount of water using the original dye concentration. For each run, careful steps were taken to minimize frost accumulation on the dyed surfaces so that effects due to variation in net surface concentration were minimized. The surface of the dyed ice was tested to determine the surface concentration after freezing; we found no significant change.

(c) *Data Acquisition*

Immediately after each set of collisions, a sample that consists of the ice surface at the point of contact is collected by scraping the surface with a scalpel blade. When measuring mass transferred to the ice brick instead of to the ball, the ice brick is removed and its surface is scraped in an identical manner. Each of the sample scrapings amounts to about 0.1 ml of water, which is usually diluted to about 1.0 ml of volume with purified water to provide the sample size required for the fluorimeter. The dilution of the sample need not be precisely the same for each run as any deviation from 1.0 ml is accounted for in the final analysis. Each sample is examined in the Spex fluorimeter which scans the emission at 90° to the incident radiation (optimal excitation for fluorescein occurs at 320 nm). The area under each fluorescent emission peak thus acquired is proportional to the concentration of dye in each sample. Comparing this with data from reference solutions of known concentrations (Fig. 1) gives an accurate determination of how much transferred dye is in the sample. Measurements of the dye transfer were made as a function of the number of collisions over the range 2–300.

(d) *Data Reduction*

A typical data plot acquired from the Spex fluorimeter is shown in Fig. 2. The

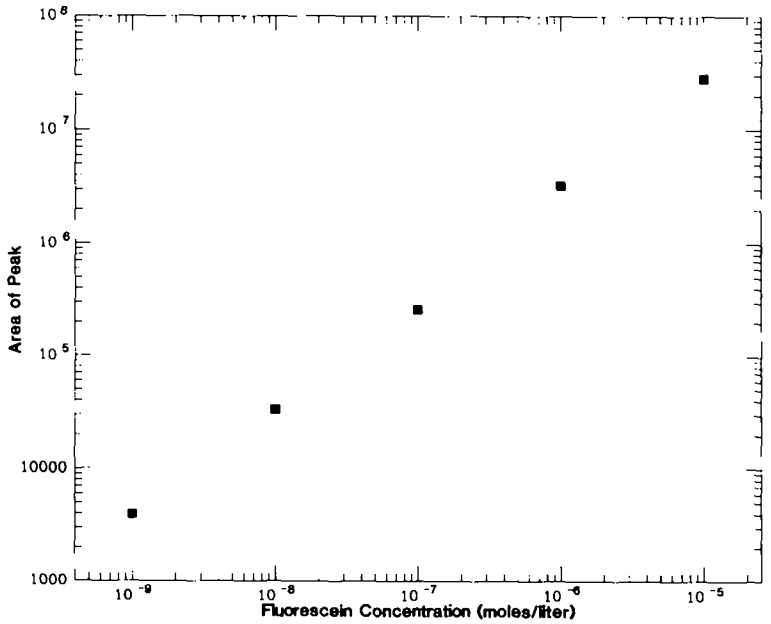

FIG. 1. Peak areas calculated by the fluorimeter data reduction routine versus dye concentration. Our data reduction hinges on this linear relation.

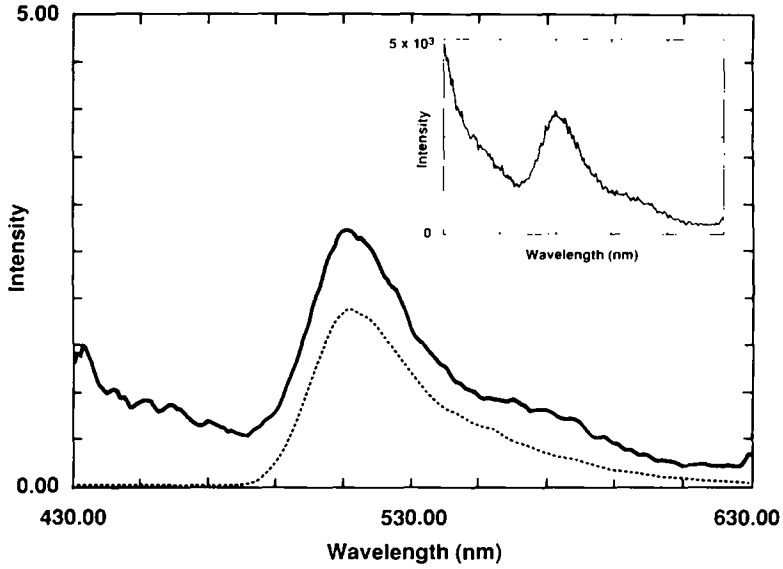

FIG. 2. Reduced data peak from the inset data (solid line) compared with a fluorescein reference peak of 10^{-8} moles per liter (dotted line). Inset: Raw data peak from 125 collisions of roughened ice. Note large sloping background due to the fluorescence of the disposable polystyrene cuvette.

disposable sample cuvettes, themselves, have a fluorescence peak at 415 nm, but a reference scan of this is saved in computer memory and is subtracted from the raw data plots. Once a raw plot of data is taken (inset, Fig. 2), bracket concentrations of reference dye are scanned. For the example illustrated in Fig. 2, the reference concentrations were 10^{-8} and 10^{-7} moles per liter. In some cases, the data are convolved with a 9-pixel smoothing filter on the Spex Datamate computer. This last step is only necessary when the signal is at very low levels. The filter helps to separate a peak trend from surrounding background and thus maximize the signal-to-noise ratio. This filter was applied to data presented in Fig. 2. On runs of 2–20 collisions, it was essential to smooth the data this way. In Fig. 2, a fluorescein reference peak (10^{-8} moles per liter) is also shown for comparison.

Using the measurement of the transferred dye in the sample, the original dye concentration, C_0, and the sample volume, V (in ml), we can calculate the effective amount of mass, μ (in g), that has been transferred from the dyed surface to the undyed surface from the equation

$$\mu = \frac{C_s}{C_0} V, \tag{1}$$

where C_s is the concentration of the sample, and the density of water is taken to be 1 g/ml. This equation has yielded the collection of data illustrated in Figs. 3–5.

To estimate the error in the data plots, an integration of background noise across a range identical to that of the sample peak is taken. The area thus measured represents a measurement of the errors in the areas under the sample curves and rarely exceeded 10% of the sample values (consistent with photon statistics). This error is then propagated through Eq. (1) to produce a measured error in μ. Errors seen in Figs. 3–5 also include the difference in values resulting from the variance of the reference concentrations due to fluctuations in fluorimeter performance. The differences due to the comparison of the data with two slightly different references (an artifact of both fluorimeter performance and very slight varia-

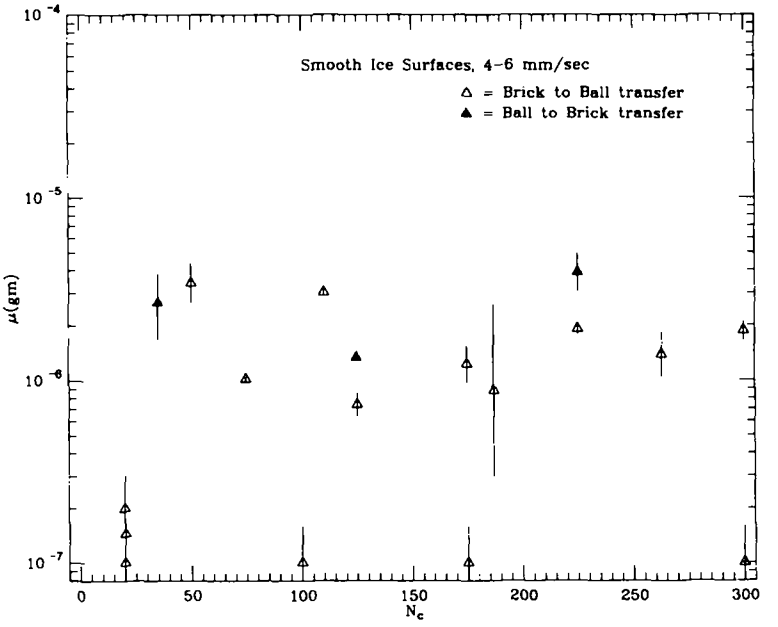

FIG. 3. The mass equivalent of the dye transferred in collisions with very smooth surfaces for velocities of 0.4 to 0.6 cm sec^{-1} as a function of the number of collisions N_c.

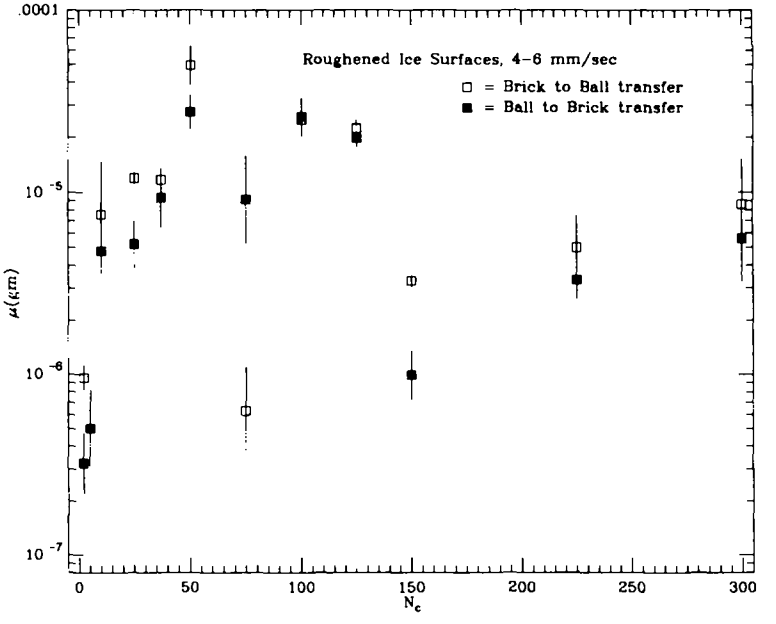

FIG. 4. The mass equivalence of the dye transferred in collisions with roughened ice surfaces for velocities from 0.4 to 0.6 cm sec^{-1} as a function of N_c.

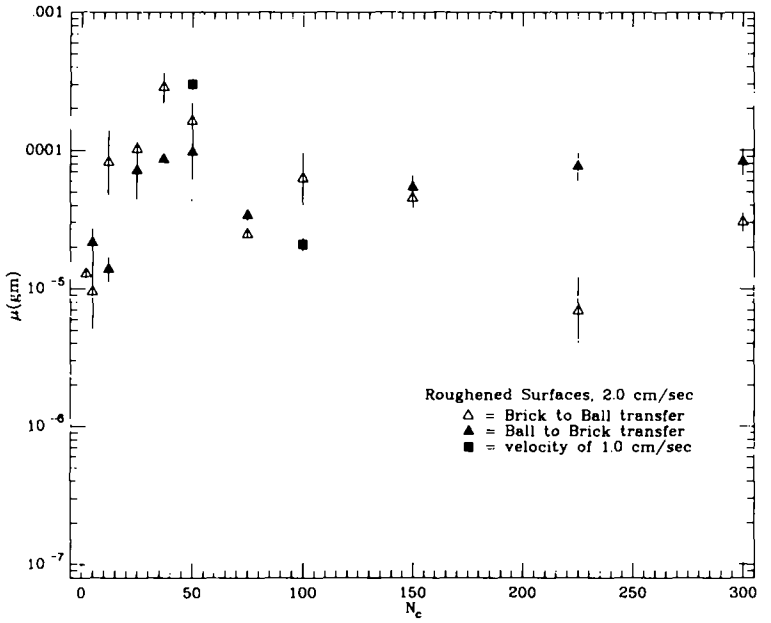

FIG. 5. Roughened ice data acquired at 2.0 cm sec^{-1}. Note that the general dependence of log μ vs log N_c is similar to that of previous data sets, but shifted to higher μ.

tions in dye concentrations over time) is also accounted for in the displayed error bars.

III. EXPERIMENTAL DATA AND THEIR IMPLICATIONS

(a) *A Brief Summary of the Data*

Sets of data were collected using ice spheres with two different macroscopic surface properties. The effective mass transfer (μ) as a function of the number of collisions, N_c, for smooth ice particles at velocities of 0.4 to 0.6 cm sec^{-1} sec is summarized in Fig. 3. The scatter in the data indicates that dye transfer is an essentially random process. Each point in Fig. 3 represents a particular ice sphere and the scatter may be a result of varying surface conditions, such as varying thickness of microscopic frost layers or fracture separated by a characteristic length scale on the order of 0.1 mm. For small N_c, μ increases linearly with N_c. For $N_c > 30$, μ attains an asymptotic value, $\sim 10^{-6}$ g, with a considerable amount of scatter. Experimentally, within this range of the scatter, the dye transferred to the ice brick from a dyed ball is equal to that transferred to the ice ball from a dyed brick.

We also obtained data for collisions between particles with roughened surfaces. In this case, no two sets of rough surfaces could present identical initial conditions in the experiment so a certain amount of additional scatter is expected in the data. This property is well illustrated by the experimental values of μ vs N_c (Fig. 4) for collisions between roughened ice particles at v = 0.4 to 0.6 cm sec^{-1}. For $N_c < 30$, μ once again attains an asymptotic value $\sim 10^{-5}$ g which is an order of magnitude larger than the corresponding value for smooth particles.

To explore velocity dependence of the mass transfer process, measurements were made of μ for roughened ice particles with a collisional velocity of 2.0 cm sec^{-1}. The results in Fig. 5 indicate a behavior similar to those in Figs. 3 and 4. The asymptotic value of μ is about an order of magnitude

greater than that of the roughened ice data at 0.5 cm sec^{-1}. The asymptotic values of μ for various impact velocities are plotted in Fig. 6. Within the scatter, there is a clear indication that the asymptotic values of μ increase with the impact velocity.

(b) A Model for Mass Transfer

We now interpret the data in Figs. 3–5 with a model for the detailed dye transfer process. For discussion purposes, the particle which initially contains dye is referred to as particle 1 and that which is initially dye-free as particle 2. Exchange in this section refers to the total mass that moves in both directions from (1) to (2) and from (2) to (1). Transfer refers to the difference in mass that moves from (1) to (2) to that from (2) to (1). In an exchange, there may be no net transfer. Our model is based on four postulates: (1) During each collision, the contact region on each particle is being compressed. Depending on the impact velocity, there is a total amount of material, Δm_i, for each particle, in the compressed region, a fraction of which participates in the transfer or exchange process. Over many collisions, all the molecules in the "exchangeable volume" may be transferred back and forth between the particles. (2) During a typical encounter, a relatively small and approximately constant fraction, f_c, of the "exchangeable volume" of a particle is actually transferred. The fraction for each of the two colliding particles need not be equal. (3) After each collision, the newly transferred material is thoroughly and uniformly mixed in the "exchangeable volume." (4) The net amount of material transferred may be much smaller than the amount that is being exchanged.

Qualitatively, postulates (1), (2), and (3) would provide the basic properties for small N_c, whereas postulates (1) and (4) would lead to the $\mu - N_c$ relationship for large N_c. For small N_c, the material transferred from particle 1 would contain a much larger dye concentration than the material transferred from particle 2 so that there is a net transfer of dye molecules from particle

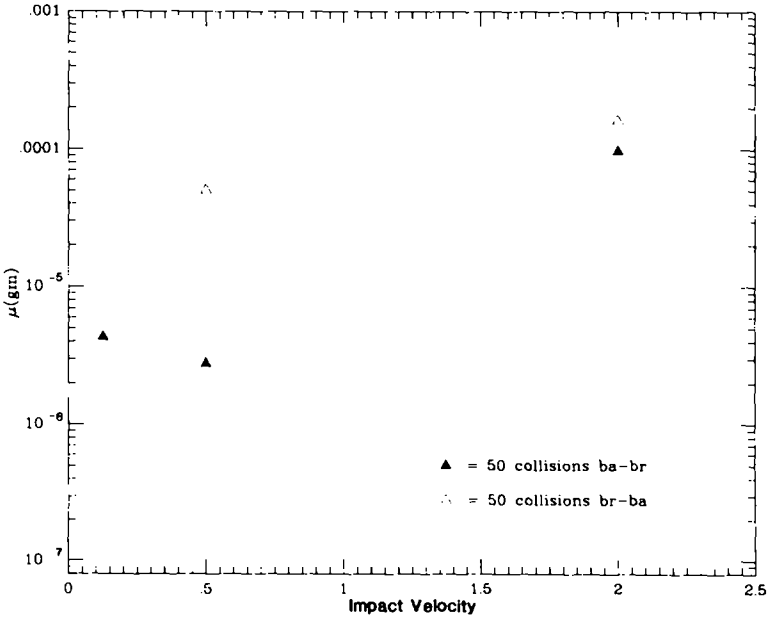

FIG. 6. Mass transfer as a function of velocity at a set number of collisions. Despite the scatter, a definite (and expected) slow upward trend is apparent.

1 to particle 2 during the initial collisions. After many collisions, the dye concentration in the "exchangeable volume" of particles 1 and 2 becomes comparable so that the net rate of dye transfer is reduced to zero. The number of collisions required for μ to reach this asymptotic limit is determined by f_c. Assuming the experiments are done for several cases with identical initial conditions, variation in the initial growth rate is determined by the constancy of f_c as well as how well the transferred material is mixed in the exchangeable volume. Finally, the asymptotic value of μ is $\sim 0.5\ \Delta m_1$ when Δm_1 and Δm_2 are comparable.

(c) Applications to Data Analysis

In order to quantitatively evaluate the above model and deduce some useful constraints on the mean value and fluctuation amplitude of mass transfer, we construct a Monte Carlo numerical simulation. In this scheme, two types of molecules, say red and blue, are initially segregated into two homogeneous boxes; i.e., all the blue molecules are contained in box 1 and red molecules in box 2. The total numbers of red (N_r) and blue (N_b) molecules are usually held constant but in some special cases are allowed to vary with N_c. During each collision, a fraction, $f_1 + g_1(\Lambda - 1)$, randomly selected molecules are transferred from box 1 to box 2, whereas $f_2 + g_2(\Lambda - 1)$ molecules are transferred from box 2 to box 1. The model parameters, f_1, f_2, g_1, and g_2 are usually held constant, but in some testing cases they are allowed to vary with N_c. The function Λ (with values between 0 and 2) provides uniformally distributed random numbers and it is introduced to provide some fluctuation. The molecules in a box are chosen at random and therefore the composition transferred during a given collision is proportional to the relative molecular concentration in the box from which they are removed.

In the first set of simulations, we set $N_r = 1000$, $N_b = 1000$, $g_1 = g_2 = 0$. Three different cases with $(1.1) f_1 = f_2 = 0.01$; $(1.2) f_1 = f_2 = 0.04$; and $(1.3) f_1 = f_2 = 0.07$ are considered. The number of red molecules in box 1, N_1, is plotted in Fig. 7a as a function of the number of collisions, N_c. For the first few collisions, N_1 increases by $\sim f_2 N_r$ per collision so that the mass exchange rate can be easily determined. Assuming a similar linear approximation for the data in Figs. 3–5 we obtain the following mass exchange rate: $<10^{-7}$ g per collision for smooth ice particles, 3×10^{-7} g per collision for roughened ice, and 3×10^{-6} g per collision for the high velocity collisions. The slopes of the lines from 0 to 40 collisions were quite uncertain and resulted in an error on these estimates of about 30 to 50%. With the present apparatus, it is not possible to directly measure the mass transferred in a single low velocity collision because these values are usually below the sensitivity of the experiment. This extrapolation of the available data was the only path to single collision measurements. The results, therefore, are likely to represent an upper limit on the transfer of mass per collision.

In our numerical simulations, N_1 reaches an asymptotic value, $N_a \sim 500$, for these three cases. The number of collisions, δN, required for N_1 to increase to say 70% of N_a decreases with f_2. In order for $\delta N \sim 20$–30, as indicated by the experimental data, $f_c \sim 0.05$. The asymptotic value for the dye concentration μ also indicates that the mass of the exchangeable volume for these three experimental cases is 2×10^{-6}, 2×10^{-5}, and 10^{-4} g, respectively. For the smooth particle case, the mass of the exchangeable volume is comparable to that of the compressed volume as deduced through Hertz's model. Due to the increases in the contact area and the fractures in the crystal structure, the exchangeable volume for the roughened particles is much larger. This property is consistent with the smaller coefficient of restitution for the roughened particles (Paper 1). Although the roughened surface may become compacted, a significant mass exchange rate can persist for at least 20–30 collisions.

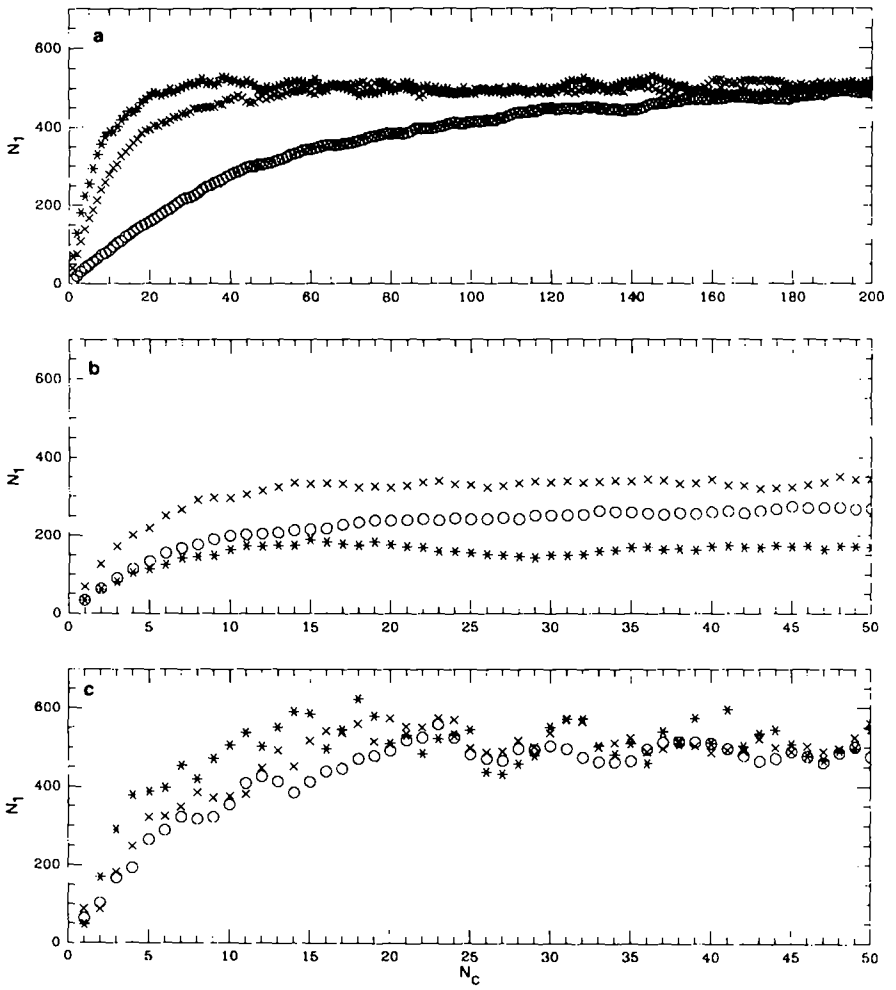

FIG. 7. Numerically simulated mass exchange process. In cases (a), $N_r = N_b = 1000$. The ○, ×, and * symbols represent models 1.1, 1.2, and 1.3, respectively. In cases (b), N_r and N_b are not generally equal. The ○, ×, and * symbols represent models 2.1, 2.2, and 2.3, respectively. In cases (c), we introduce fluctuations in the fraction of exchangeable volume being transferred during each encounter. The ○, ×, and * symbols represent models 3.1, 3.2, and 3.3, respectively. The values of N_r, N_b, f_1, f_2, g_1, and g_2 are given in the text.

In the second set of simulations we again set $g_1 = g_2 = 0$. The results presented in Fig. 7b are for three different cases: (2.1) $N_r = N_b = 500$ and $f_1 = f_2 = 0.07$; (2.2) $N_r = N_b = 1000$, $f_1 = 0.14$, and $f_2 = 0.07$; and (2.3) $N_b = 1000$, $N_r = 500$, $f_1 = 0.14$, and $f_2 = 0.07$. These results indicate that the asymptotic value of $N_1 \sim N_r f_2/(f_1 + f_2)$ and δN decreases with f_2 and increases with f_1. We note from these results that (1) the comparable results for the asymptotic value of μ from ice ball to brick, and to that from ice brick to ball, imply that the exchangeable volume in both ice ball and brick is similar. (2) Comparable values of δN for ice ball to brick and for brick to ice ball implies that $f_c \sim 0.05$ for both ice ball and brick.

Our numerical results indicate that the asymptotic value of N_1 is maintained in the limit of constant f_1 and f_2; i.e., mass is being

exchanged on a continuum basis. This result implies that postulate 4 can lead to results compatible with experimental data. Nevertheless, we cannot yet rule out the possibility that the asymptotic values of N_1 are reached because of a gradual reduction in f_1 and f_2. Data presented in Paper 1 indicate that the coefficient of restitution increases with N_c for small N_c and then attains an asymptotic value suggesting that freshly frosted surfaces are compacted in 5 to 20 collisions, depending on the velocity and the radius of curvature. Similar data for the spherical particles used in these experiments, at a velocity of 5 mm/sec, are plotted in Fig. 8. These data suggest that f_c may decrease somewhat in the first few collisions as the contact regions become more compacted. This possibility may be particularly relevant to the case for the roughened particles.

Experimental data in Figs. 3–5 indicate considerable amounts of scatter in the asymptotic values of μ. We point out that each experimental point is from a different particle. The large scatter may simply be the result of a varying amount of frost and the different initial surfaces. In Figs. 7a and b, there are also some fluctuations in the asymptotic values of N_1 which are due to statistical noise in the limiting number of particles. The amplitude of the fluctuation may be increased with finite values for g_1 and g_2. The results of the third set of simulations are plotted in Fig. 7c for three additional cases: (3.1) $N_r = N_b = 1000, f_1 = f_2 = 0.07$, and $g_1 = g_2 = 0.04$; (3.2) $N_r = N_b = 1000, f_1 = f_2 = 0.07$, and $g_1 = g_2 = 0.07$; and (3.3) $N_r = N_b = 1000, f_1 = f_2 = 0.14$, and $g_1 = g_2 = 0.1$. We note that in order to model the large scale fluctuations in Figs. 3–5, variation in f_c may be comparable to the value of f_c itself especially for the roughened balls. Such large fluctuation in f_c may also be the underlying reason for the fluctuation in the coefficient of restitution for various impact velocities (see Paper 1).

IV. DISCUSSIONS

The data in Paper 1 and the results presented above indicate that the surface structure of particles in planetary rings ba-

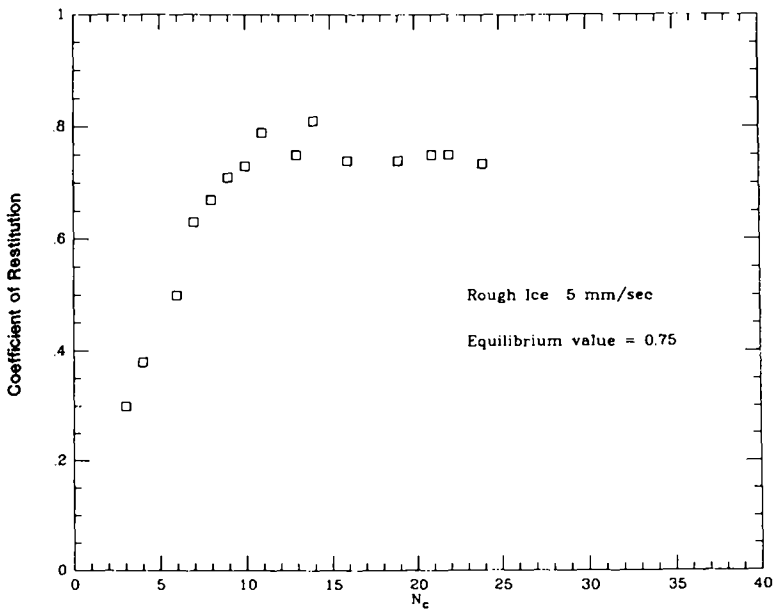

FIG. 8. The coefficient of restitution as a function of N_c for a roughened ice sphere and brick. More details are given in Paper 1.

sically determines both the mass exchange rate and the coefficient of restitution. If the ring particles are hard spheres (Goldreich and Tremaine 1978), the particle collisions would be essentially elastic and little mass exchange would take place during the collisions. If the particles' surface is highly fractured or coated with thick frosts, similar to the "dynamical ephemeral bodies" (Weidenschilling *et al.* 1984), the collisions would be very inelastic and the mass exchange rate during each collision would be relatively large. There is little direct observational data on the actual surface properties of the ring particles. Based on our experimental data, we construct some constraints for the particles' properties.

(*a*) *Impact Craters and Granulations*

Our experimental results indicate that the mass of the exchangeable volume for particles with regular crystal-structure surfaces is comparable to the compressible volume estimated from the simple Hertz model. In this case, the collisions induce microscopic impact craters with a radius $r \sim (R_p \Delta m/\rho_p)^{1/4}$, where R_p and ρ_p are the particles' radius and density, respectively. Taking Δm to be the measured asymptotic values of μ, we find $r \sim 0.03$ cm which is comparable to those estimated values of r in Section II(b). However, if the surface of the particles has a roughness with a characteristic length-scale, l_c, comparable to r, Δm is determined by l_c rather than R_p. A distribution in the values of l_c would introduce considerable fluctuations in Δm. When the experimental value of Δm ($\sim 10^{-5}$ g) for roughened particles is used, we find $l_c \sim 0.03$ cm. Associated with this relatively large Δm is a greater amount of energy dissipation. Thus, for roughened particles, ε is significantly less than unity and has a range of values (see Fig. 8) for a particular impact velocity. Since the dynamical properties of the ring particles are sensitively determined by ε, it is important to cast some constraints on the actual nature of the particles' surface.

(*b*) *Evolution of the Surface Structures*

The surface structure of ring particles determines the amount of energy loss during each collision and therefore the coefficient of restitution. For example, in order to damp density waves in Saturn's rings over the observed distance scales from where they were excited, ε appropriate for particles with relatively smooth surfaces is needed (Shu *et al.* 1986). If a large fraction of the particles in the waves have roughened surfaces, the velocity dispersion of the particles would be damped by the low effective ε. For low velocity dispersion, the density waves would not be dispersed. However, particles may be continually fractured and eroded by micrometeoroid impact (Morfill *et al.* 1983) and coated with frost as they accrete micron-size ice grains (Borderies *et al.* 1984). For a typical particle revolving around Saturn at an angular frequency Ω, the rate of accretion of grains is

$$\dot{M}_a \sim R_p^2 \rho_g \Omega f_s \int \tau_g(\lambda) d\lambda,$$

where ρ_g (~ 1 g cm^{-3}) is the density of the grain, and $\tau_g(\lambda)$ is the optical depth of grains with size λ. Voyager data indicate that $\tau_g < 0.1$ for grains with $\lambda \sim 10^{-5}$ to 10^{3} cm (Cuzzi *et al.* 1984). More recent analyses indicate that $\tau_g \sim 0.01$ (Dones 1987). The sticking probability $f_s < 1$ is a very uncertain quantity. Accretion of millimeter or larger particles is also possible. If these particles are loosely bound to the centimeter-size accretors, they may be displaced during subsequent collisions and provide additional energy dissipation. If these particles are firmly attached to the accretors, the accretion of these particles is less important than the continual frost coating and formation of fractures with $l_c \sim r \sim 10^{-2}$ cm in reducing the effective value of ε (see Section II(b)).

Nevertheless, a relatively large value of ε may be maintained because accompanying the fracture and accretion process, the contact regions are also being compacted by

collisions. Our experimental results indicate that a minimum number, N_m (>30), of collisions over the same location are needed to compact the total exchangeable volume. Thus the rate of compactification is

$$\dot{M}_c \sim N_m^{-1} \Delta m \Omega \tau_p,$$

where τ_p is the average optical depth of the ice particles. The observed particle-size distribution implies that for a typical particle, its most likely collisional partners have a size ~1 cm so that τ_p is referred to these particles.

A collisional equilibrium may be established in which $\dot{M}_a \sim \dot{M}_c$ for particles with a characteristic radius, R_c, given by

$$R_c = \left(\frac{\Delta m \tau_p}{N_m \rho_g f_s \int \tau_g(\lambda) d\lambda} \right)^{1/2}.$$

Assuming f_s is of order unity and applying reasonable estimates for the other model parameters, we find R_c to be the order of a centimeter. For particles with $R_p \gg R_c$, accretion and erosion are more effective than compactification so that their surface would be covered with irregular structure and fractures. Collisions with these particles would be more dissipative so that they may have relatively low velocity dispersion and form a monolayer structure. These expectations are consistent with Voyager's data (Cuzzi *et al.* 1984) which suggest that the largest (meter-size) particles are restricted to a monolayer.

The surface of particles with $R_p < R_c$ would be regular and smooth. Relatively small amounts of mass are transferred and $\varepsilon \sim 1$ for low velocity collisions. These particles would have relatively large velocity dispersion and ring scale height. The size distribution of the ring particles suggests that the larger (meter-size) particles contain most of the mass whereas the smaller (centimeter-size) particles contain most of the area. Collisions are more frequent among the smaller particles and their evolution may determine the observed structure of the ring. For example, the structure of the density wave may be determined by kinematic properties of the smaller particles. The requirement for a relatively large velocity dispersion in this case (Shu *et al.* 1986) is consistent with our conclusion that the smaller particles may have a smooth and harder surface and therefore have relatively large values of ε.

Voyager's data also indicate a considerable difference in the radial distribution of 1 cm vs 4 cm particles (see Fig. 10, Cuzzi *et al.* 1984). This may be due to the difference in the angular momentum transfer rate which is determined by the velocity dispersion, and therefore ε, of the particles. Since R_c lies approximately in this range, it may be possible that the 1-cm particles are more elastic and have a higher dispersion velocity than the 4-cm particles.

(c) *Evolution of Size Distribution*

The surface-structure differences between the large and small particles can affect the evolution of the size distribution. For particles with $R_p > R_c$, the exchangeable volume is relatively large. When they collide with other large particles, the net amount of material transferred may be smaller than that being exchanged because these particles have an uncompacted surface. However, they collide more frequently with smaller particles which for $R_p < R_c$ have compacted surfaces. During collisions, the net mass transferred will be primarily from large particles to small particles. In this case, the net amount of mass transferred from the large particles to the small particles is a significant fraction of that in the exchangeable volume. Because they are more abundant, small and smooth-surface particles with $R_p < R_c$ collide more frequently with particles similar to themselves. During these collisions, the net amount of mass transfer is caused by stochastic fluctuations in the mass exchange process and is a small fraction of the exchangeable volume.

This collisionally induced mass exchange process may lead to evolution for the particle-size distribution. The characteristic erosion time scale for the large particles may be $\tau_e \sim \rho_p R_p^3/(\Delta m \Omega \tau_r)$, where τ_r is the optical depth of the ring. For particles with R_p from a few to a few hundred centimeters, τ_e may range from a few hundred years to the age of the Solar System. It is of interest to note that if there is a significant population of small grains, the collisionally induced erosion process would be less efficient than the accretion process. Thus, either the large particles continue to grow or there is some other erosion process such as micrometeorite bombardment (Durisen 1984) which is controlling the particle-size evolution.

If R_c is relatively large, the small particles seldom collide with large and roughened surface particles. In this case, their size evolution is determined by the stochastic mass redistribution among themselves. Significant evolution would only be induced on a time scale $\sim(\rho_p R_p^3/\Delta m)^2/(\Omega\tau_r)$ which may be comparable to the age of the Solar System. This time scale can be shortened considerably if R_c is relatively small.

The qualitative discussions presented above are preliminary interpretations and simple applications to Saturn's rings. Obviously much additional investigation is needed to verify some of these hypotheses and proposals. For example, the data obtained here are for direct collisions. The effects of surface structure may be even greater once grazing collisions are considered. Nevertheless, these results indicate that the experimental data can be used effectively to cast constraints and deduce implications on the dynamics of planetary rings.

ACKNOWLEDGMENT

This work was supported in part by NASA Grant NAGW-590.

REFERENCES

BORDERIES, N., P. GOLDREICH, AND S. TREMAINE 1984. Unsolved problems in planetary ring dynamics. In *Planetary Rings* (R. Greenberg and A. Brahic, Eds.), pp. 713–734. Univ. of Arizona Press, Tucson.

BRIDGES, F., A. HATZES, AND D. LIN 1984. Structure, stability and evolution of Saturn's rings. *Nature (London)* **309**, 333–335.

CUZZI, J. N., J. J. LISSAUER, L. W. ESPOSITO, J. B. HOLBERG, E. A. MAROUF, G. L. TYLER, AND A. BOISCHOT 1984. Saturn's rings: Properties and processes. In *Planetary Rings* (R. Greenberg and A. Brahic, Eds.), pp. 73–199. Univ. of Arizona Press, Tucson.

DONES, L. 1987. Ph.D. thesis, University of California, Berkeley, CA.

DURISEN, P. H. 1984. Transport effects due to particle erosion mechanisms. In *Planetary Rings* (R. Greenberg and A. Brahic, Eds.), pp. 416–446. Univ. of Arizona Press, Tucson.

GOLDREICH, P., AND S. TREMAINE 1978. The velocity dispersion in Saturn's rings. *Icarus* **34**, 227–239.

HATZES, A. P., F. G. BRIDGES, AND D. N. C. LIN 1988. Collisional properties of ice spheres at low impact velocities. *Mon. Not R. Astron. Soc.* **213**, 1091–1116.

HOBBS, P. V. 1974. *Ice Physics*, p. 837. Oxford Univ. Press, London.

MAROUF, E. A., G. L. TYLER, H. A. ZEBKER, R. A. SIMPSON, AND V. R. ESHLEMAN 1983. Particle size distributions in Saturn's rings from Voyager 1 radio occultation. *Icarus* **54**, 189–211.

MORFILL, G. E., H. FECHTIG, E. GRÜN, AND C. K. GOETZ 1983. Some consequences of meteoroid impacts on Saturn's rings. *Icarus* **55**, 439–447.

SHU, F. H., L. D. UNES, J. J. LISSAUER, C. YUAN, AND J. N. CUZZI 1986. Nonlinear spiral density waves: Viscous damping. *Astrophys. J.* **299**, 542–573.

WEIDENSCHILLING, S. J., C. R. CHAPMAN, D. R. DAVIS, AND R. GREENBERG 1984. Ring particles: Collective interactions and physical nature. In *Planetary Rings* (R. Greenberg and A. Brahic, Eds.), pp. 367–415. Univ. of Arizona Press, Tucson.